# Molecular Dynamics Study of the Mechanical Properties of Nickel Nanoparticles with a Nanocrystalline Structure

Gennady Poletaev *, Alexander Semenov, Yuriy Bebikhov, Roman Rakitin

Posted Date: 7 April 2026

doi: 10.20944/preprints202604.0301.v1

Keywords: molecular dynamics; nanoparticle; deformation; nanocrystalline structure; strength

 doi:10.20944/preprints202604.0301.v1



*Article*

# Molecular Dynamics Study of the Mechanical Properties of Nickel Nanoparticles with a Nanocrystalline Structure

**Gennady Poletaev [1,*], Alexander Semenov [2,3], Yuriy Bebikhov [2] and Roman Rakitin [4]**

[1] Polzunov Altai State Technical University, Lenin Av. 46, 656038 Barnaul, Russia
[2] Polytechnic Institute of North-Eastern Federal University, Tikhonova Str. 5, 678170 Mirny, Russia
[3] Institute of Molecule and Crystal Physics UFRC RAS, Oktyabrya Av. 151, 450075 Ufa, Russia
[4] Altai State University, Lenin Av. 61, 656049 Barnaul, Russia
* Correspondence: gmpoletaev@mail.ru

**Abstract**

Using the molecular dynamics method, the compression of nickel nanoparticles with a nanocrystalline structure at low temperatures was simulated. The influence of the nanoparticle size (from 2 to 20 nm) and the average grain size within it (from 2 to 8 nm) on the compressive strength and on the strain at which the maximum stress is reached was investigated. In addition, the stability of the nanocrystalline structure of the nanoparticles was studied as a function of temperature and grain size. It is shown that the smaller the diameter of the nanocrystalline particle, the higher the compressive strength and the strain at which the maximum stress is reached. A decrease in grain size leads to a reduction in compressive strength, which is associated with the main mechanism of plastic deformation of nanocrystalline nanoparticles, namely grain boundary sliding. At the first stage of deformation, the entire particle structure typically rotates until the maximum value of the stress vector projection onto the preferred slip plane is reached, which, in the case of a nanocrystalline structure, is determined by the mutual orientation of the grain boundaries. Grain boundaries elongated approximately along a single plane represent, in this case, the preferred slip plane.

**Keywords:** molecular dynamics; nanoparticle; deformation; nanocrystalline structure; strength

## 1. Introduction

Metallic nanoparticles (NPs) possess a unique combination of physical, chemical, and optical properties [1], which makes them promising for such fields as microelectronics, optoelectronics and plasmonics [2,3], chemical catalysis, the development of gas sensors [4,5], as well as medicine and biology [6,7]. Regarding their mechanical properties, it has been established that metallic NPs often exhibit significantly higher mechanical properties compared to their bulk counterparts [8–12], which makes them attractive for use as fillers in composite materials and for improving the tribological properties of lubricants [11]. Using nanoindentation techniques, it has been experimentally found that the strength of single-crystal nanoparticles under compression can reach gigantic values, up to several tens of GPa [8–10]. For example, in [10], a strength of 34 GPa was recorded when compressing single-crystal nickel nanoparticles with a diameter of 210 nm.

At present, it is known that the compressive strength of single-crystal NPs increases as their size decreases, which has been demonstrated both experimentally and by computer simulations [10,13–18]. In some studies, for example [19–22], it is assumed that this effect is associated with the decrease in the volume required for a dislocation to form as the size of a single-crystal particle decreases. In other words, it is implied that the size effect on the compressive strength of NPs is a feature specific only to particles with a single-crystal structure, and that nanocrystalline and amorphous particles should not exhibit a similar behavior. However, the data obtained in studies devoted to the

 doi:10.20944/preprints202604.0301.v1



simulation of the compression of amorphous particles are inconsistent: in [23,24], for example, the particle size had almost no effect on the strength within the error margin, whereas in [25], as well as in our previous work [18], it was found that the strength of particles with an amorphous structure increases as their size decreases.

The next interesting property that has been discovered during the deformation of nanoparticles is the increase in fracture toughness with decreasing particle size [26]. In the experimental study [10], during nanoindentation of nickel particles, the maximum compressive stress, for example, was reached at a strain of 10–20%. In [27], using high-resolution transmission electron microscopy, it was shown that silver NPs smaller than 10 nm under compression at room temperature behave similarly to liquid droplets. In [28–30], it was found that nanoparticles made of comparatively very brittle materials, such as silicon or magnesium oxide, can exhibit plastic behavior under compression.

In addition to particles with a crystalline structure, particles with a high degree of atomic structure disorder, amorphous or nanocrystalline, are currently of great interest [31–34]. They possess high stored energy values, unique electronic structures, and a range of useful mechanical properties. Nanoparticles with a nanocrystalline structure can be obtained, for example, by cooling molten NPs at sufficiently high rates of $10^{10}$–$10^{12}$ K/s [35–37]. At such cooling rates, the suppression of the growth of some grains by others does not have time to occur, resulting in the formation of numerous fine grains with an average size of just a few nanometers. The primary mechanism of plastic deformation in the case of a nanocrystalline structure is not the formation and glide of dislocations, so-called intragranular sliding, but rather the shear of grains relative to each other along grain boundaries, i.e., grain boundary sliding. In this case, a reduction in the average grain size typically leads to a decrease in the strength of the nanocrystalline material – the so-called inverse Hall-Petch relationship [38,39]. Nevertheless, the effect of grain size on the mechanical properties of metallic nanoparticles remains poorly studied. Moreover, no studies of the compression of nanoparticles with a nanocrystalline structure have been conducted previously.

This work is devoted to the investigation, using molecular dynamics simulations, of the mechanical properties of spherical nickel NPs with a nanocrystalline structure under compressive deformation at low temperatures. Particular attention is focused on the influence of the average grain size, as well as the size of the nanoparticle itself, on its compressive strength and fracture toughness. Additionally, the stability of the nanocrystalline structure of nickel NPs is examined as a function of temperature and grain size. The features of the deformation process are also analyzed. The choice of nickel particles as an example is motivated by their wide practical applications. Nickel exhibits high corrosion resistance, enhanced plasticity and ductility, and serves as an effective catalyst. The simulation of nanoparticle compression in this work is conducted at low temperatures primarily due to the main objective of the study – to elucidate the effect of average grain size on the mechanical properties of nanoparticles, while an increase in temperature, as is known, leads to the intensification of recrystallization, i.e., unstable grain sizes during the simulation.

## 2. Description of the Model

Interatomic interactions in the molecular dynamics model were described using a many-body potential developed in [40] based on the embedded atom method, taking into account the experimental properties of pure nickel: cohesive energy, lattice parameter, and elastic constants. In [40], it was shown that this potential successfully reproduces a wide range of other nickel properties, including the energy characteristics of various defects, the phonon spectrum, and thermal expansion. The potential we used has proven itself well in various molecular dynamics simulations, including plastic deformation, the formation and glide of dislocations, structural-phase transformations, and self-diffusion [40–42]. Previously, it has already been used by us in studies of the melting and crystallization of nickel nanoparticles [35,43], as well as in investigations of the mechanical properties of single-crystal and amorphous nanoparticles [18].

Previously, in [35], we demonstrated that nickel nanoparticles with a nanocrystalline structure can be obtained by cooling molten NPs at sufficiently high rates on the order of $10^{10}$–$10^{12}$ K/s.

 doi:10.20944/preprints202604.0301.v1



Moreover, by varying the cooling rate, it is possible to control the average grain size and, accordingly, the stored energy – with an increase in cooling rate, the final NP structure contains more defects and the magnitude of potential energy stored in the defects increases [35]. However, this method of obtaining a nanocrystalline structure in a molecular dynamics model has a drawback consisting in a large scatter of grain sizes, as well as the presence of a high density of extraneous defects.

In this work, we aimed to create grains within the particle of approximately the same size. This was necessary to study the effect of grain size on the mechanical properties of the nanoparticle. It should be noted that, for example, in the inverse Hall-Petch relationship describing the influence of grain size on the strength of a material with a nanocrystalline structure, the average grain size is involved [38,39]. Nevertheless, a scatter in grain size obviously introduces some error into the results, and if it is possible to minimize it in the model, it is better to do so. The procedure for creating the nanoparticle was as follows. At the first stage, in the computational cell of a perfect nickel crystal shaped as a rectangular parallelepiped, the centers of future grains were determined depending on the specified average grain size. These centers were positioned relative to each other akin to the nodes of a large lattice with FCC packing – in this case, the distance between the nearest grain centers was the same. Next, the structure around each center within spheres of diameter 0.8 times the specified grain size (nearest distance between centers) was rotated in space by random angles. As a result, the majority of grain boundaries turned out to be high-angle. After that, with the structure inside the spheres fixed, the remaining structure (regions near the grain boundaries) was melted by heating to a temperature of 2500 K and then crystallized by holding it for 300 ps at a temperature of 1500 K. Subsequently, the fixation of the grain center structures was released, and relaxation was performed for an additional 20 ps at 100 K, followed by cooling to 0 K. The resulting structure consisted of approximately equal-sized grains whose shapes were close to that of a truncated octahedron. The grain sizes varied from 2 to 8 nm. Grains smaller than 2 nm, as will be shown below, were too unstable – under deformation or heating, recrystallization occurred accompanied by grain growth.

At the next stage, a spherical nanoparticle of the specified diameter was cut out from the obtained computational cell with a nanocrystalline structure. The particle diameter varied from 2 to 20 nm. Obviously, when cutting out the particle, the average grain size became smaller due to the truncation of some grains – for such particles, the average size was recalculated accordingly. After cutting out the spherical particle, structural relaxation was performed again for 20 ps at 100 K, followed by cooling to 0 K. The low temperature and short duration of relaxation were chosen to avoid premature recrystallization at this stage, as it would lead to an increase in the average grain size.

Examples of particles with a nanocrystalline structure with grain sizes of 2.9 and 4.8 nm are shown in Figure 1. Free space was simulated around the particle. The particle was placed in the center of a computational cell in the form of a rectangular parallelepiped. During structural relaxation at the nanoparticle creation stage, periodic boundary conditions were applied along all axes (in this case, boundary conditions could generally not be used, but periodic conditions guarantee the conservation of a constant number of atoms $N$ in the computational cell). Maintaining a constant temperature $T$ during relaxation was achieved using the Nosé-Hoover thermostat. No barostat was used – the particle could freely change its volume and shape due to structural rearrangements, and the pressure $P$ was zero. Thus, at the structural relaxation stage, the $NPT$ canonical ensemble was used. The molecular dynamics time integration step was 1 fs.

 doi:10.20944/preprints202604.0301.v1



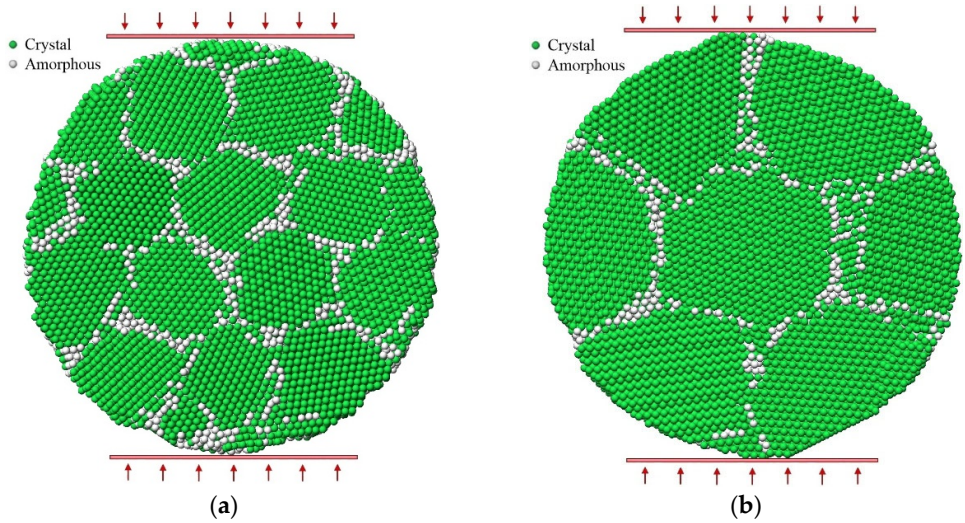


**Figure 1.** Cross-section of a nanocrystalline particle with a diameter of 12 nm and average grain size of: **(a)** 2.9 nm; **(b)** 4.8 nm.

The grain boundaries in the created nanoparticles were predominantly high-angle and of mixed type due to the random distribution of the crystal grain orientations. Low-angle boundaries, as can be seen from the particle cross-section examples in Figure 1, were noticeably fewer – they differ from high-angle ones by their comparatively lower density of white atoms in the figures, whose nearest environment does not match any crystal lattice. It is known that high-angle boundaries have higher formation energy compared to low-angle ones, and they are characterized by lower activation energy values for grain boundary diffusion, grain boundary sliding, and boundary migration [36–39].

Uniaxial compression of the nanoparticle was simulated by moving virtual flat boundaries on both sides of the particle at a constant rate (Figure 1). Atoms interacted with the moving virtual boundaries absolutely elastically. Compressive stress was determined as the ratio of the total force acting on the virtual flat boundaries from the atoms to the contact area. A similar method of simulating nanoparticle compression was used in most works performed using molecular dynamics. The approach of the virtual boundaries was typically modeled at rates from 10 to 50 m/s at an initial temperature of 0 K [15,16,44,45]. Compression rates in this range are achievable in real experiments, nevertheless, in [18], when studying the mechanical properties of single-crystal nickel nanoparticles, we, in particular, showed that with increasing deformation rate, the compressive strength of nanoparticles increases, while it decreases with increasing temperature. At the same time, in [18], it was noted that at rates below 10 m/s, the effect of compression rate on nanoparticle strength decreased and was less pronounced. In this work, the studies were conducted at a compression rate of 10 m/s and an initial temperature of 0 K. The initial temperature of 0 K was used for several reasons. First, the main goal of this study was to elucidate the effect of average grain size on the mechanical properties of the nanoparticle, whereas an increase in temperature, as will be shown below, leads to the intensification of recrystallization and grain growth, especially in the case of relatively small grain sizes. Second, most simulations of nanoparticle compression have been performed at an initial temperature of 0 K, making it easier to compare the obtained data with the results of other authors. Third, lowering the temperature allows for a clearer analysis of structural transformations during deformation due to reduced thermal noise. No thermostat was used during compression simulation in this work. The temperature could increase during deformation. This was done to avoid introducing artificial restrictions on atomic motion during deformation processes.

## 3. Results and Discussion

The obtained nanoparticle structures, containing grains just a few nanometers in size and the corresponding high density of grain boundaries and other defects, are obviously unstable at elevated

 doi:10.20944/preprints202604.0301.v1



temperatures. Before conducting the main investigations in this work, an analysis of the stability of the obtained particle structures as a function of temperature was performed. The analysis was carried out based on the magnitude of the average potential energy per atom in the particle after simulation at a specified constant temperature for 250 ps followed by cooling to 0 K. The change in the average atomic energy well indicates the intensity of structural transformation – in this case, recrystallization – as a decrease in the average atomic energy occurs due to a reduction in the defect density, primarily grain boundaries, in the particle. The simulation duration of 250 ps was chosen because the main computer experiments on nanoparticle compression had the same duration (during which the particle was deformed by approximately 20%).

Figure 2 shows the dependencies of the average atomic energy on temperature in a 12 nm diameter particle after simulation for 250 ps followed by cooling to 0 K for different initial grain sizes. Dashed lines on the figure indicate energy levels corresponding to the initial structures, with the energy level for a single-crystal particle also shown additionally. It is clearly seen that the smaller the initial grain size, the higher the average atomic energy, which, as already mentioned, is explained by the higher density of grain boundaries.

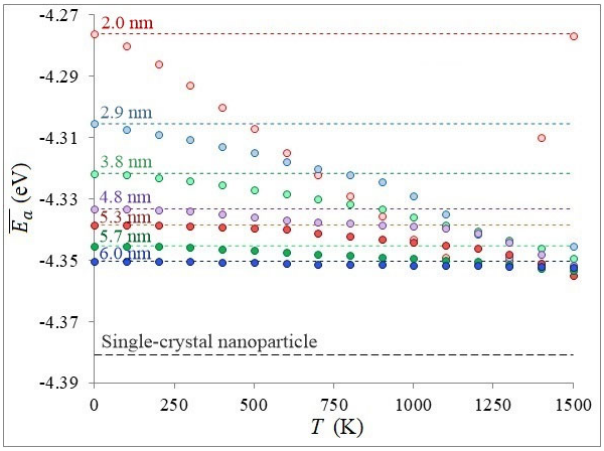


**Figure 2.** Average potential energy of an atom in a nanoparticle with a diameter of 12 nm as a function of temperature and initial average grain size after simulation for 250 ps and subsequent cooling to 0 K.

As seen in Figure 2, with increasing temperature, the average potential energy per atom after simulation for 250 ps decreases, indicating recrystallization during the simulation. Moreover, the smaller the initial grain size, the more intense the recrystallization, which is apparently explained by the comparatively greater stored energy in the case of smaller grain sizes. Using the energy levels shown in the figure, it is possible to estimate which structure corresponds to the structure after simulation at a given temperature. For example, a nanoparticle with an initial average grain size of 2.0 nm begins to correspond in average energy magnitude after simulation for 250 ps to a grain size of 2.9 nm only at a temperature of 500 K, while a nanoparticle with an initial average grain size of 2.9 nm corresponds to a structure with 3.8 nm grains at approximately 700 K.

For the particle with an initial grain size of 2 nm, at temperatures above 1400 K, the average energy values were significantly higher than the main trend – this is associated with the melting and amorphization of the particle. As shown, for example, in [46,47], as well as in our works [48,49], in the case of very small grain sizes, with increasing grain boundary density and, accordingly, stored energy, the melting temperature decreases.

The main conclusion that can be drawn from the conducted analysis is that at low temperatures close to 0 K, at which the compression simulation is planned to be performed in this work, the average grain size in the considered range of values remains relatively stable during the anticipated simulation time.

 doi:10.20944/preprints202604.0301.v1



Obviously, with further increase in simulation duration beyond 250 ps, the recrystallization process will continue, and the more intense it will be, the higher the temperature and the smaller the average grain size. Due to grain growth during this recrystallization, a gradual slowdown in recrystallization rates over time should be expected until a certain state is reached, characterized by low stored energy and low defect density.

Figure 3 presents examples of strain-stress dependences for the compression of a 12 nm diameter nanocrystalline nickel nanoparticle with three different grain sizes: 2.5, 3.8, and 5.7 nm. A characteristic feature of all presented dependences is the presence of several local peaks associated with structural adjustment in the contact patches where the load is applied. It is clearly seen that the compressive strength, i.e., the maximum stress achieved during nanoparticle compression, increases with increasing average grain size. For the examples shown in Figure 3: for 2.5 nm grain size – approximately 7.4 GPa, for 3.8 nm – 10.3 GPa, for 5.7 nm – 14.0 GPa. For comparison, in [10], nanoindentation of single-crystal nickel particles with the regular shape of truncated octahedra yielded strength values from 10 GPa for 880 nm particles to 34 GPa for 210 nm particles. In [17], performed using molecular dynamics simulation, the compressive strength of truncated octahedron-shaped nickel nanoparticles ranged from 20 GPa for 20 nm diameter particles to 35 GPa for 5 nm diameter particles. The strength of particles with a nanocrystalline structure proves to be lower than that of single-crystal particles due to the high density of grain boundaries and other defects present in them.

The second notable feature in Figure 3 is the relatively ductile, non-brittle nature of particle deformation – the maximum stress values are reached at relatively large strain values of 6–10%. However, this is not a feature of the nanocrystalline structure in this case – such ductile deformation behavior was also observed during compression of crystalline nanoparticles in real experiments [10,27].

It should be noted that the stress-strain dependences obtained in the model were unfortunately characterized by rather large errors and significant oscillations in stress values. These errors increased with decreasing nanoparticle size and typically ranged from 0.7 GPa for 20 nm particles to approximately 1.6 GPa for 2 nm particles in the region of peak stress values. As particle size decreased, the contribution of errors in calculating the contact patch areas grew, along with the influence of atomic structure discreteness – during atomic structure rearrangement near the virtual boundaries compressing the particle, smaller particles exhibited stronger fluctuations in the computed contact patch areas. Secondly, the particle shape itself deviated more frequently from an ideal sphere at the start of simulation as it became smaller. The formation of faceted shapes instead of spherical ones for relatively small particles is associated with free energy minimization. The third factor is the temperature rise during deformation due to the release of kinetic energy from structural transformations. This temperature increase leads to additional thermal atomic vibrations, which in turn amplify the errors caused by the two aforementioned factors. All these causes act in concert, making it difficult to isolate the influence of any single one. One way to mitigate them in this case is to increase the number of simulations, including creating more nanoparticles of various sizes with different grain boundary orientations and using different compression axes for the nanoparticles.

 doi:10.20944/preprints202604.0301.v1



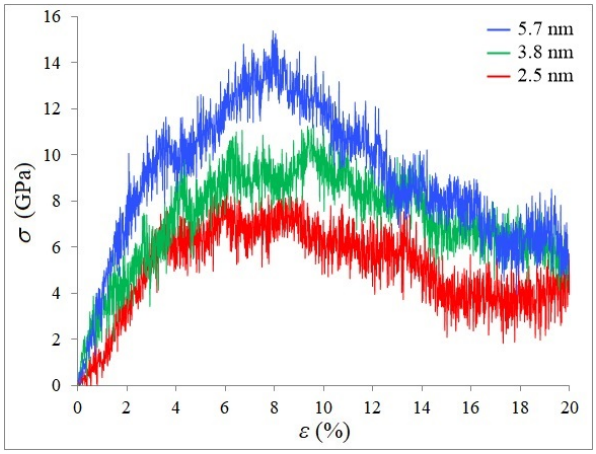


**Figure 3.** Stress-strain dependencies during the compression of a nanocrystalline nickel nanoparticle with a diameter of 12 nm and three different grain sizes.

Figure 4 shows the dependencies of the maximum compressive stress $\sigma_{max}$ and the associated strain $\varepsilon_{max}$ on the average grain size $\delta$ for a nanoparticle with a diameter of 12 nm. When obtaining the dependencies in Figure 4, 13 nanoparticles with a diameter of 12 nm and different grain sizes from 2 to 6 nm were used. Uniaxial compression of each particle, for a more comprehensive analysis, was performed twice along mutually perpendicular *x* and *y* axes, that is, a total of 26 data points were obtained for Figures 4*a* and 4*b*. In Figure 4*a*, which depicts the dependence $\sigma_{max}(\delta)$, it is clearly seen that the strength decreases as the average grain size diminishes: from 14 GPa at $\delta$=6 nm down to approximately 6 GPa at $\delta$=2 nm. This behavior is explained by the fact that, for a nanocrystalline structure with grain sizes of only a few nanometers, plastic deformation occurs mainly not through the formation and movement of dislocations within grains, but rather through grain boundary sliding. At the same time, the reduction in grain size and the increase in the density of grain boundaries lead, respectively, to a decrease in the energy required to carry out plastic shear and to the facilitation of plastic deformation. A similar effect is observed in bulk materials with a nanocrystalline structure and an average grain size typically below 10 nm – the so-called inverse Hall-Petch relationship [38,39].

At the same time, for the deformation at which the maximum stress $\varepsilon_{max}$ was reached, no clear dependence on the grain size was observed in our work (Figure 4*b*). For all the grain sizes considered, the value of $\varepsilon_{max}$ remained within the range of 6–10%. This is an interesting result that contradicts the similar dependence observed in bulk nanocrystalline materials, where plasticity and fracture ductility increase as the average grain size decreases. Apparently, in this case, the ductility of fracture and the value of $\varepsilon_{max}$ are more strongly influenced by a feature inherent to any nanoparticles, related to the relatively small area of the contact patches and processes associated with the structural rearrangement near them.

 doi:10.20944/preprints202604.0301.v1



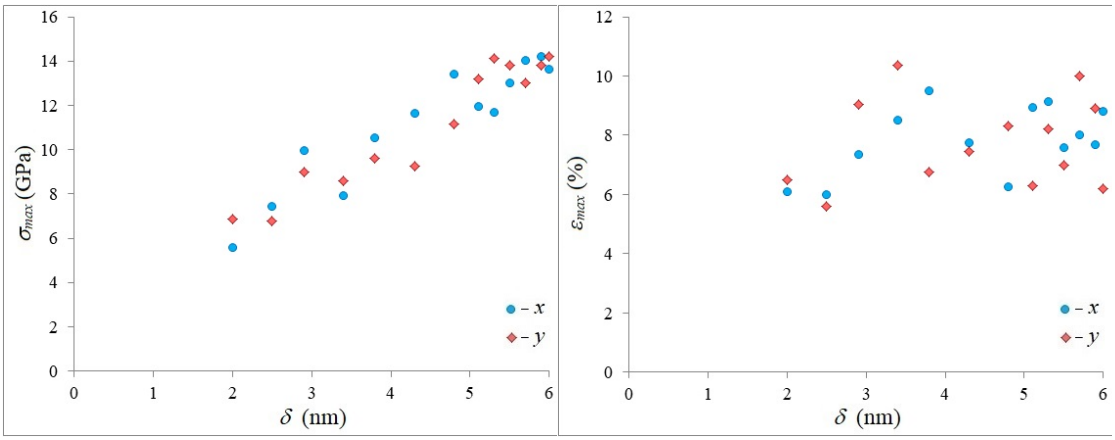


(**a**) (**b**)

**Figure 4.** Dependences of maximum compressive stress **(a)** and associated strain **(b)** on the average grain size for a nanoparticle with a diameter of 12 nm.

Figure 5*a* shows the dependence of the maximum compressive stress $\sigma_{max}$ on the nanoparticle size $d$, containing grains with an average size of approximately 3 nm (for particles smaller than 6 nm, the grain size was actually already less than 3 nm). To study the influence of particle size on mechanical properties, 24 nanoparticles of different diameters were used. For each particle, uniaxial compression was performed along two different axes, $x$ and $y$, resulting in a total of 48 data points for Figures 5*a* and 5*b*.

As mentioned above, several researchers currently believe that the effect of crystalline particle size on their compressive strength is related to the reduction in available volume for dislocation sources as the size of single-crystal particles decreases [19–22]. However, as seen in Figure 5*a*, for particles with a nanocrystalline structure, where deformation occurs primarily not through dislocations but through grain boundary sliding, a clear increase in strength with decreasing particle size is also observed. Even for particles smaller than 6 nm, where the average grain size was actually already less than 3 nm, the strength increased as the particle size decreased.

It can be observed that as the diameter of nanoparticles decreases, the scatter of strength values determined in the model increases, which is explained by the growing error in stress calculation with decreasing nanoparticle size. This, in turn, is caused by an increase in the error of contact patch area determination, as well as by the increasing influence of particle shape and surface relief on strength in the case of small particles. Small deviations of particle shape from spherical or the presence of atomic steps on the surface led to noticeable deviations in the obtained values.

Figure 5*b* shows the dependence of the strain $\varepsilon_{max}$ at which the maximum strength was reached on the nanoparticle size $d$. As can be seen, $\varepsilon_{max}$ increases as the particle size decreases, which is consistent with the results of other authors [26–30]. The obtained values of $\varepsilon_{max}$ range from 5% for particles with a diameter of 20 nm to 20% for 2 nm particles. For comparison, in the experimental study [10], for single-crystal nickel particles, the maximum stress was reached at strains of 10–20%, while in the work [50], performed using molecular dynamics simulations, for nickel nanoparticles with a diameter of 10 nm, the maximum stress was reached at compressions of 5–15%.

 doi:10.20944/preprints202604.0301.v1



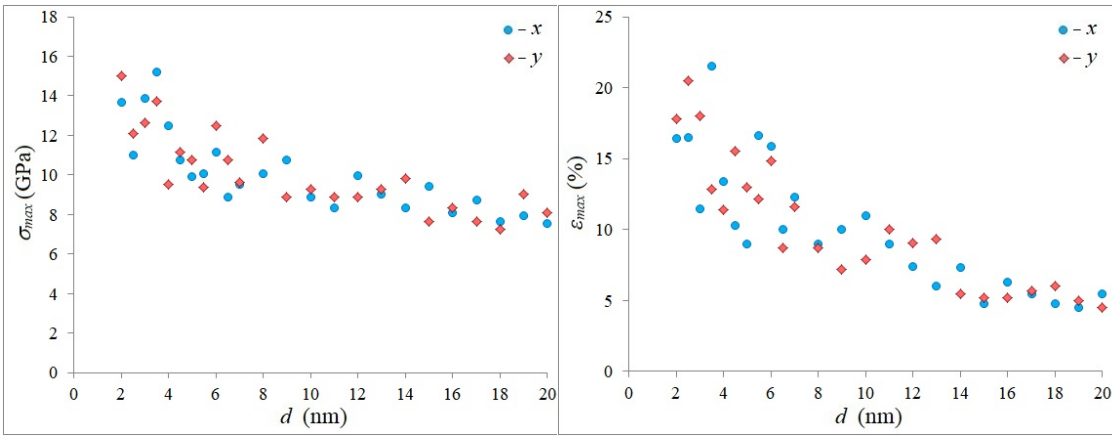


(**a**) (**b**)

**Figure 5.** Dependences of maximum compressive stress **(a)** and associated strain **(b)** on the nanoparticle size with an average grain size of 3 nm.

Figure 6 shows cross-sections of particles with a diameter of 12 nm and grain sizes of 2.9 and 4.8 nm after deformations of 12% and 10%, respectively. The initial structure of the same particles before deformation is shown in Figure 1. As can be seen, compression of the nanoparticles caused a rotation of the entire particle structure by approximately 9° in the case of 2.9 nm grains and by 11° in the case of 4.8 nm grains. In our previous work [18], when studying the deformation of single-crystal nickel particles, it was also noted that a rotation of the entire particle structure occurs at the initial stage of deformation. Typically, this rotation is more pronounced for relatively small particles and continues until the projection of the stress vector on the slip plane reaches its maximum – that is, when the angle between the slip plane and the compression direction reaches about 45°. After that, for the single-crystal particle in [18], the stage of dislocation nucleation from the contact spots followed. However, in the case of a nanocrystalline structure, as in the present work, where the grain size is only a few nanometers, dislocations, i.e., plastic slips within the grains, were almost never observed. Slips occurred predominantly along grain boundaries. In other words, the main mechanism of plastic deformation in our case was grain boundary sliding. In our case, the main mechanism of plastic deformation was grain boundary sliding; therefore, the slip plane was determined not by crystallographic orientation but by the orientation of the grain boundaries. The grain boundaries, elongated approximately along one plane, represented the preferential slip plane in this case. The grain boundaries along which the preferred slip plane formed were generally close to a plane oriented at a 45° angle to the compression axis. It is evident that sliding occurred more readily along high-angle boundaries compared to low-angle ones.

It should also be noted that, as in the case of compression of amorphous particles in [18], in the present work a phenomenon of structural densification near the contact patches was also observed for nanocrystalline particles, along with reorientation of the structure so that the most densely packed atomic planes of the (111) type became parallel to the contact patch plane. This effect became progressively more pronounced with increasing deformation.

Therefore, the following main stages of deformation during compression of nanocrystalline nanoparticles can be distinguished. First, structure crushing occurred near the contact patches, accompanied by its densification and reorientation such that the atomic planes near the contact patches became predominantly of (111) type. Next, gradual rotation of the entire particle structure around an axis perpendicular to the compression direction took place until the projection of the stress vector onto the shear plane reached its maximum. The shear plane in this case, i.e., for the nanocrystalline structure, consisted of elongated grain boundaries roughly aligned in one plane. At the next stage, shear along them occurred in the form of grain boundary sliding.

 doi:10.20944/preprints202604.0301.v1



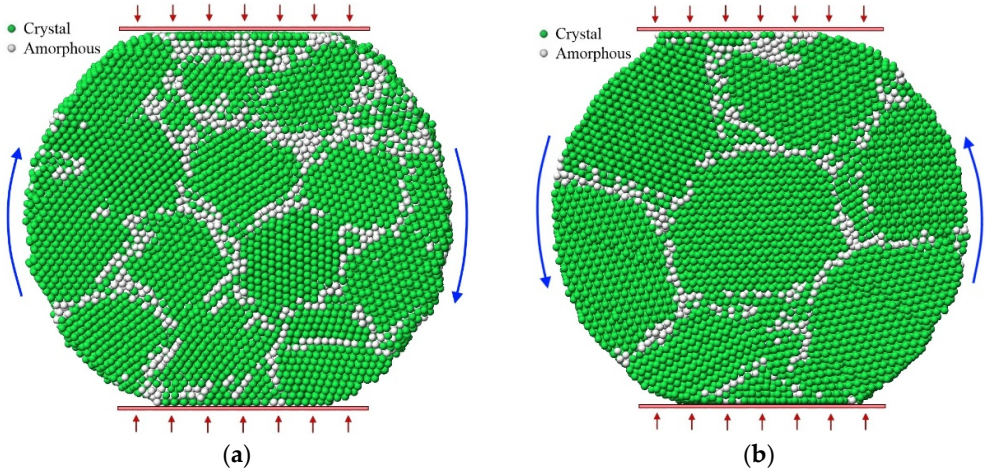


**Figure 6.** Cross-sections of nanocrystalline particles with a diameter of 12 nm at the moment of compression with an average grain size of: **(a)** 2.9 nm, strain 12%; **(b)** 4.8 nm, strain 10%.

Thus, in the present work for nanoparticles with a nanocrystalline structure, as well as for single-crystal nanoparticles in [10,13–18] and amorphous ones in [18,25], the influence of nanoparticle diameter on their strength and fracture toughness has been confirmed once again – the smaller the nanoparticle size, the higher the compressive strength and the strain value at which maximum compressive stress is reached. However, the reasons for such dependence prove to be nontrivial and may differ for the aforementioned structures, involving several factors simultaneously. For example, according to [19–22], for single-crystal nanoparticles, the volume required for dislocation formation and development is important; for amorphous ones, as shown in [18], densification and strengthening, often combined with partial crystallization, occur near the load application sites. In the case of nanoparticles with a nanocrystalline structure, whose compression was simulated here for the first time, the deformation mechanism becomes even more complex due to the simultaneous action of several processes: grain boundary sliding, grain rotation, and recrystallization. Plastic shears formed within the nanoparticle volume not through dislocation formation and propagation, but via cooperative sliding along a set of grain boundaries.

Regarding the influence of the average grain size on the mechanical properties of nanocrystalline nanoparticles, which was studied for the first time in the present work, it has been established that compressive strength decreases with decreasing average grain size. For example, for a particle with a 12 nm diameter, the strength dropped more than twofold when the grain size decreased from 6 to 2 nm – from 14 to 6 GPa. At the same time, for the strain value at which maximum stress was reached, our work revealed no pronounced dependence on grain size at the same nanoparticle size.

## 4. Conclusions

Molecular dynamics simulations were used to simulate the compression of spherical nanocrystalline nickel nanoparticles at low temperatures. The influence of the nanoparticle size and the average grain size within it on the compressive strength and on the strain at which maximum stress is reached was investigated. Additionally, the stability of the nanocrystalline structure of the nanoparticles was studied as a function of temperature and grain size. Features of plastic deformation in nanoparticles with a nanocrystalline structure were identified. The study yielded the following conclusions.

1. The intensity of recrystallization and structural changes that lead to a decrease in the average potential energy of an atom in the nanoparticle increases as the average grain size decreases and temperature rises. However, at the low temperatures at which the compression simulation of the nanoparticles was conducted, the average grain size within the considered range remained relatively stable.

 doi:10.20944/preprints202604.0301.v1



2. The compressive strength (the maximum compressive stress) of the particles decreases with a reduction in their average grain size. For a nickel particle with a diameter of 12 nm, the strength dropped by more than half as the grain size decreased from 6 to 2 nm – from 14 to 6 GPa.

3. As the size of nanocrystalline nanoparticles decreases, their compressive strength increases, similar to the case of single-crystal particles. For particles with a nanocrystalline structure and an average grain size of approximately 3 nm, the strength increased from 8 GPa for particles with a diameter of 20 nm to 15 GPa for 2 nm particles, with the grains in the latter case being even smaller than 3 nm.

4. With decreasing nanocrystalline particle size, the value of deformation at which the maximum stress is achieved during compression of nanoparticles also increases. For the considered nanocrystalline particles, it ranged from 5% for particles with a diameter of 20 nm to 20% for 2 nm particles.

5. Plastic deformation in nanoparticles with a nanocrystalline structure occurred predominantly through grain boundary sliding. At the initial stage, the entire particle structure typically rotated until the projection of the stress vector onto the preferential slip plane reached its maximum. In the case of the nanocrystalline structure, this preferential slip plane was determined by the mutual orientation of the grain boundaries. The grain boundaries, elongated roughly along one plane, as a rule, represented the preferential slip plane.

**Author Contributions:** Investigation, data curation, G.P., A.S., Y.B. and R.R.; writing–original draft preparation, G.P.; conceptualization, writing–review and editing, G.P., A.S. and Y.B. All authors have read and agreed to the published version of the manuscript.

**Funding:** This research received no external funding.

**Data Availability Statement:** Data will be made available upon request.

**Conflicts of Interest:** The authors declare no conflicts of interest.

## References

1. Dekker Encyclopedia of Nanoscience and Nanotechnology, 3rd ed; ed. by J.A. Schwarz, S.E. Lyshevski, C.I. Contescu; CRC Press: Boca Raton, USA, 2014; 4200 p.
2. Humbert, C.; Noblet, T.; Dalstein, L.; Busson, B.; Barbillon, G. Sum-frequency generation spectroscopy of plasmonic nanomaterials: a review. *Materials* **2019**, *12*, 836. https://doi.org/10.3390/ma12050836.
3. Mantri, Y.; Jokerst, J.V. Engineering plasmonic nanoparticles for enhanced photoacoustic imaging. *ACS Nano* **2020**, *14*, 9408–9422. https://doi.org/10.1021/acsnano.0c05215.
4. Kodama, K.; Nagai, T.; Kuwaki, A.; Jinnouchi, R.; Morimoto, Y. Challenges in applying highly active Pt-based nanostructured catalysts for oxygen reduction reactions to fuel cell vehicles. *Nat. Nanotechnol.* **2021**, *16*, 140–147. https://doi.org/10.1038/s41565-020-00824-w.
5. Mitchell, S.; Qin, R.; Zheng, N.; Perez-Ramirez, J. Nanoscale engineering of catalytic materials for sustainable technologies. *Nat. Nanotechnol.* **2021**, *16*, 129–139. https://doi.org/10.1038/s41565-020-00799-8.
6. Jain, T.K.; Morales, M.A.; Sahoo, S.K.; Leslie-Pelecky, D.L.; Labhasetwar, V. Iron oxide nanoparticles for sustained delivery of anticancer agents. *Mol. Pharm.* **2005**, *2*, 194–205. https://doi.org/10.1021/mp0500014.
7. Shim, S.Y.; Lim, D.K.; Nam, J.M. Ultrasensitive optical biodiagnostic methods using metallic nanoparticles. *Nanomedicine* **2008**, *3*, 215–232. https://doi.org/10.2217/17435889.3.2.215.
8. Carlton, C.E.; Ferreira, P.J. In situ TEM nanoindentation of nanoparticles. *Micron* **2012**, *43* (11), 1134–1139. https://doi.org/10.1016/j.micron.2012.03.002.
9. Deneen, J.; Mook, W.M.; Minor, A.; Gerberich, W.W.; Carter, C.B. In situ deformation of silicon nanospheres. *J. Mater. Sci.* **2006**, *41*, 4477–4483. https://doi.org/10.1007/s10853-006-0085-9.
10. Sharma, A.; Hickman, J.; Gazit, N.; Rabkin, E.; Mishin, Y. Nickel nanoparticles set a new record of strength. Nat. Commun. **2018**, *9*, 4102. https://doi.org/10.1038/s41467-018-06575-6.
11. Guo, D.; Xie, G.; Luo, J. Mechanical properties of nanoparticles: basics and applications. *J. Phys. D Appl. Phys.* **2014**, *47*, 013001. https://doi.org/10.1088/0022-3727/47/1/013001.

 doi:10.20944/preprints202604.0301.v1




12. Ramos, M.; Ortiz-Jordan, L.; Hurtado-Macias, A.; Flores, S.; Elizalde-Galindo, J.; Rocha, C.; Torres, B.; Zarei-Chaleshtori, M.; Chianelli, R. Hardness and elastic modulus on six-fold symmetry gold nanoparticles. *Materials* **2013**, *6* (1), 198–205. https://doi.org/10.3390/ma6010198
13. Mordehai, D.; Lee, S.-W.; Backes, B.; Srolovitz, D.J.; Nix, W.D.; Rabkin, E. Size effect in compression of single-crystal gold microparticles. *Acta Mater.* **2011**, *59* (13), 5202–5215. https://doi.org/10.1016/j.actamat.2011.04.057.
14. Han, W.-Z.; Huang, L.; Ogata, S.; Kimizuka, H.; Yang, Z.-C.; Weinberger, C.; Li, Q.-J.; Liu, B.-Y.; Zhang, X.-X.; Li, J.; Ma, E.; Shan, Z.-W. From "smaller is stronger" to "size-independent strength plateau": towards measuring the ideal strength of iron. *Adv. Mater.* **2015**, *27* (22), 3385–3390. https://doi.org/10.1002/adma.201500377.
15. Hong, Y.; Zhang, N.; Zaeem, M.A. Metastable phase transformation and deformation twinning induced hardening-stiffening mechanism in compression of silicon nanoparticles. *Acta Mater.* **2018**, *145*, 8–18. https://doi.org/10.1016/j.actamat.2017.11.034.
16. Amodeo, J.; Pizzagalli, L. Modeling the mechanical properties of nanoparticles: a review. *Comptes Rendus. Physique, Plasticity and Solid State Physics* **2021**, *22* (S3), 35–66. https://doi.org/10.5802/crphys.70.
17. Feruz, Y.; Mordehai, D. Towards a universal size-dependent strength of face-centered cubic nanoparticles. *Acta Mater.* **2016**, *103*, 433–441. http://dx.doi.org/10.1016/j.actamat.2015.10.027.
18. Poletaev, G.; Sannikov, A.; Gafner, Y.; Gafner, S.; Zorya, I. Mechanical properties of crystalline and amorphous nickel nanoparticles: molecular dynamics simulation. *J. Nanoparticle Res.* **2025**, *27*, 153. https://doi.org/10.1007/s11051-025-06354-7.
19. Kiener, D.; Minor, A.M. Source truncation and exhaustion: insights from quantitative in situ TEM tensile testing. *Nano Lett.* **2011**, *11* (9), 3816–3820. https://doi.org/10.1021/nl201890s.
20. Mompiou, F.; Legros, M.; Sedlmayr, A.; Gianola, D.S.; Caillard, D.; Kraft, O. Source-based strengthening of sub-micrometer Al fibers. *Acta Mater.* **2012**, *60* (3), 977–983. https://doi.org/10.1016/j.actamat.2011.11.005.
21. Dunstan, D.J.; Bushby, A.J. The scaling exponent in the size effect of small scale plastic deformation. *Int. J. Plast.* **2013**, *40*, 152–162. https://doi.org/10.1016/j.ijplas.2012.08.002.
22. Phani, P.S.; Johanns, K.E.; George, E.P.; Pharr, G.M. A simple stochastic model for yielding in specimens with limited number of dislocations. *Acta Mater.* **2013**, *61* (7), 2489–2499. https://doi.org/10.1016/j.actamat.2013.01.023.
23. Kilymis, D.; Gerard, C.; Pizzagalli, L. Mechanical properties of amorphous silicon nanoparticles. In: TMS 2019 148th Annual Meeting & Exhibition Supplemental Proceedings. The Minerals, Metals & Materials Series. Springer, Cham. **2019**, 1347–1354. https://doi.org/10.1007/978-3-030-05861-6_128.
24. Issa, H.K.; Taherizadeh, A.; Maleki, A. Atomistic-level study of the mechanical behavior of amorphous and crystalline silica nanoparticles. *Ceram. Int.* **2020**, *46* (13), 21647–21656. https://doi.org/10.1016/j.ceramint.2020.05.272.
25. Zhao, J.; Nagao, S.; Odegard, G.M.; Zhang, Z.; Kristiansen, H.; He, J. Size-dependent mechanical behavior of nanoscale polymer particles through coarse-grained molecular dynamics simulation. *Nanoscale Res. Lett.* **2013**, *8*, 541. https://doi.org/10.1186/1556-276X-8-541.
26. Beaber, A.; Nowak, J.; Ugurlu, O.; Mook, W.; Girshick, S.; Ballarini, R.; Gerberich, W. Smaller is tougher. *Phil. Mag.* **2011**, *91*, 1179–1189. https://doi.org/10.1080/14786435.2010.487474.
27. Sun, J.; He, L.; Lo, Y.C.; Xu, T.; Bi, H.; Sun, L.; Zhang, Z.; Mao, S.X.; Li, J. Liquid-like pseudoelasticity of sub-10-nm crystalline silver particles. *Nat. Mater.* **2014**, *13*, 1007–1012. https://doi.org/10.1038/nmat4105.
28. Issa, I.; Amodeo, J.; Rethore, J.; Joly-Pottuz, L.; Esnouf, C.; Morthomas, J.; Perez, M.; Chevalier, J.; Masenelli-Varlot, K. In situ investigation of MgO nanocube deformation at room temperature. *Acta Mater.* **2015**, *86*, 295–304. https://doi.org/10.1016/j.actamat.2014.12.001.
29. Mook, W.; Nowak, J.; Perrey, C.; Carter, C.; Mukherjee, R.; Girshick, S.; McMurry, P.; Gerberich, W. Compressive stress effects on nanoparticle modulus and fracture. *Phys. Rev. B* **2007**, *75*, 214112. https://doi.org/10.1103/PhysRevB.75.214112.
30. Gerberich, W.W.; Stauffer, D.D.; Beaber, A.R.; Tymiak, N.I. A brittleness transition in silicon due to scale. *J. Mater. Res.* **2012**, *27*, 552–561. https://doi.org/10.1557/jmr.2011.348.

 doi:10.20944/preprints202604.0301.v1




31. Liang, S.-X.; Zhang, L.-C.; Reichenberger, S.; Barcikowski, S. Design and perspective of amorphous metal nanoparticles from laser synthesis and processing. *Phys. Chem. Chem. Phys.* **2021**, *23*, 11121–11154. https://doi.org/10.1039/D1CP00701G.
32. Sun, J.; Sinha, S.K.; Khammari, A.; Picher, M.; Terrones, M.; Banhart, F. The amorphization of metal nanoparticles in graphitic shells under laser pulses. *Carbon* **2020**, *161*, 495–501. https://doi.org/10.1016/j.carbon.2020.01.067.
33. He, D.S.; Huang, Y.; Myers, B.D.; Isheim, D.; Fan, X.; Xia, G.-J.; Deng, Y.; Xie, L.; Han, S.; Qiu, Y.; Wang, Y.-G.; Luan, J.; Jiao, Z.; Huang, L.; Dravid, V.P.; He, J. Single-element amorphous palladium nanoparticles formed via phase separation. *Nano Res.* **2022**, *15*, 5575–5580. https://doi.org/10.1007/s12274-022-4173-1.
34. Qian, Y.; Silva, A.; Yu, E.; Anderson, C.L.; Liu, Y.; Theis, W.; Ercius, P.; Xu, T. Crystallization of nanoparticles induced by precipitation of trace polymeric additives. *Nat. Commun.* **2021**, *12*, 2767. https://doi.org/10.1038/s41467-021-22950-2.
35. Poletaev, G.M.; Bebikhov, Y.V.; Semenov, A.S.; Molecular dynamics study of the formation of the nanocrystalline structure in nickel nanoparticles during rapid cooling from the melt. *Mater. Chem. Phys.* **2023**, *309*, 128358. https://doi.org/10.1016/j.matchemphys.2023.128358.
36. Kumar, K.S.; Van Swygenhoven, H.; Suresh, S. Mechanical behavior of nanocrystalline metals and alloys. *Acta Mater.* **2003**, *51*, 5743–5774. https://doi.org/10.1016/j.actamat.2003.08.032.
37. Meyers, M.A.; Mishra, A.; Benson, D.J. Mechanical properties of nanocrystalline materials. Prog. Mater. Sci. **2006**, *51*, 427–556. https://doi.org/10.1016/j.pmatsci.2005.08.003.
38. Quek, S.S.; Chooi, Zh.H.; Wu, Zh.; Zhang, Y.W.; Srolovitz D.J. The inverse Hall-Petch relation in nanocrystalline metals: A discrete dislocation dynamics analysis. *J. Mech. Phys. Solids.* **2016**, *88*, 252-266. https://doi.org/10.1016/j.jmps.2015.12.012.
39. Naik, S.N.; Walley, S.M. The Hall-Petch and inverse Hall-Petch relations and the hardness of nanocrystalline metals. *J. Mater. Sci.* **2020**, *55*, 2661-2681. https://doi.org/10.1007/s10853-019-04160-w.
40. Purja Pun, G.P.; Mishin, Y. Development of an interatomic potential for the Ni-Al system. *Phil. Mag.* **2009**, *89*, 3245–3267. https://doi.org/10.1080/14786430903258184.
41. Levchenko, E.V.; Ahmed, T.; Evteev, A.V. Composition dependence of diffusion and thermotransport in Ni-Al melts: a step towards molecular dynamics assisted databases, Acta Mater. **2017**, *136*, 74–89. https://doi.org/10.1016/j.actamat.2017.06.056.
42. Poletaev, G.M.; Bebikhov, Yu.V.; Semenov, A.S.; Starostenkov M.D. Self-diffusion in melts of Ni-Al and Ti-Al systems: molecular dynamics study. *Letters on Materials* **2021**, *11* (4), 438–441. https://doi.org/10.22226/2410-3535-2021-4-438-441.
43. Poletaev, G.M.; Gafner, Y.Y.; Gafner, S.L. Molecular dynamics study of melting, crystallization and devitrification of nickel nanoparticles. *Letters on Materials* **2023**, *13* (4), 298–303. https://doi.org/10.22226/2410-3535-2023-4-298-303.
44. Bian, J.; Zhang, H.; Niu, X.; Wang, G. Anisotropic deformation in the compressions of single crystalline copper nanoparticles. *Crystals* **2018**, *8* (3), 116. https://doi.org/10.3390/cryst8030116.
45. Bian, J.J.; Yang, L.; Niu, X.R.; Wang, G.F. Orientation-dependent deformation mechanisms of bcc niobium nanoparticles. *Phil. Mag.* **2018**, *98* (20), 1848–1864. https://doi.org/10.1080/14786435.2018.1459059.
46. Xiao, S.; Hu, W.; Yang, J. Melting temperature: from nanocrystalline to amorphous phase. *J. Chem. Phys.* **2006**, *125* (18), 184504. https://doi.org/10.1063/1.2371112.
47. Noori, Z.; Panjepour, M.; Ahmadian, M. Study of the effect of grain size on melting temperature of Al nanocrystals by molecular dynamics simulation. *J. Mater. Res.* **2015**, *30*, 1648–1660. https://doi.org/10.1557/jmr.2015.109.
48. Poletaev, G.M.; Sitnikov, A.A.; Bebikhov, Yu.V.; Semenov, A.S. Influence of mean grain size and excess energy on the melting temperature of nanocrystalline aluminum. *Letters on Materials* **2025**, *15* (2), 77–83. https://doi.org/10.48612/letters/2025-2-77-83.
49. Poletaev, G.; Rakitin, R.; Bebikhov, Y.; Semenov, A. Molecular dynamics study of melting initiation at tilt grain boundaries depending on their misorientation angle in aluminum. *Phys. Scr.* **2025**, *100*, 015988. https://doi.org/10.1088/1402-4896/ad9ef8.

 doi:10.20944/preprints202604.0301.v1



50. Goryaeva, A.M.; Fusco, C.; Bugnet, M.; Amodeo, J. Influence of an amorphous surface layer on the mechanical properties of metallic nanoparticles under compression. *Phys. Rev. Mater.* **2019**, *3*, 033606. https://doi.org/10.1103/PhysRevMaterials.3.033606.